Enhancement of quadripartite quantum correlation via phase-sensitive cascaded four-wave mixing process

Huanrong He,[1] Shengshuai Liu,[1,4,*] and Jietai Jing[1,2,3,4,5,†]

[1]*State Key Laboratory of Precision Spectroscopy, Joint Institute of Advanced Science and Technology, School of Physics and Electronic Science, East China Normal University, Shanghai 200062, China*

[2]*CAS Center for Excellence in Ultra-intense Laser Science, Shanghai 201800, China*

[3]*National Laboratory of Solid State Microstructures, Nanjing University, Nanjing 210093, China*

[4]*Chongqing Key Laboratory of Precision Optics, Chongqing Institute of East China Normal University, Chongqing 401120, China*

[5]*Collaborative Innovation Center of Extreme Optics, Shanxi University, Taiyuan, Shanxi 030006, China*

(Received 2 March 2022; revised 29 October 2022; accepted 17 January 2023; published 2 February 2023)

Multipartite quantum correlation is important for both fundamental science and quantum information processing. Its enhancement is critical to improve the performance of physical systems. Therefore, it is of great practical significance to study the enhancement of multipartite quantum correlation. Here, we theoretically investigate a scheme for enhancing quadripartite quantum correlation by utilizing a phase-sensitive cascaded four-wave mixing (CFWM) process. We find that the intensity-difference squeezing (IDS) among the four output beams generated by the phase-insensitive CFWM process can be largely enhanced by introducing the phase-sensitive CFWM process. We also find that our phase-sensitive CFWM process can be used to generate intensity-sum squeezing (ISS), which cannot be generated by the phase-insensitive CFWM process. Moreover, we find that the maximum squeezing value of ISS is equal to that of IDS when the intensity gains of the three four-wave mixing processes are equal in the phase-sensitive cascaded scheme. In the end, we discuss the effects of the losses and the phase fluctuations on the squeezing values of our phase-sensitive CFWM process and the corresponding phase-insensitive CFWM process with the same intensity gains. It can be seen that the squeezing enhancement of our phase-sensitive CFWM process holds also in presence of the losses and the phase fluctuations. Our results pave the way for experimental implementation and may find applications in quantum metrology and quantum communication.

DOI: 10.1103/PhysRevA.107.023702

I. INTRODUCTION

Multipartite quantum correlation has attracted extensive attention due to its importance in both fundamental science [1,2] and quantum technologies [3–5]. A number of different techniques for its generation have been widely studied. For instance, in the continuous-variable (CV) regime, the most well-established method for generating multipartite quantum correlation is to mix the independent single-mode squeezed states on a linear beam-splitter network [6–9]. Considering the scalability for future applications, some groups have experimentally followed another promising approach which generates multiple optical modes in the nonlinear process to avoid the use of a complicated linear beam-splitter network [10–12]. Recent advances related to this aspect include the generation of the ultra-large-scale CV cluster state in both the time [13–15] and frequency [16,17] domains.

All schemes mentioned above are based on optical parametric oscillators (OPOs), which are well-studied nonlinear quantum systems for producing quantum correlated beams. Besides OPOs, the four-wave mixing (FWM) process with a double-Λ energy-level configuration in a ^{85}Rb vapor cell has been proved to be an efficient way to generate quantum correlated beams [18] due to its strong nonlinearity and natural spatial separation of the output beams. This system was used in several recent advances, such as quantum imaging [19–23], the tunable delay of Einstein-Podolsky-Rosen entanglement [24], the implementation of an SU(1,1) nonlinear interferometer [25–29], ultrasensitive measurement of microcantilever displacement [30], and the generation of orbital-angular-momentum multiplexed CV bipartite entanglement [31]. Moreover, the FWM process has been experimentally demonstrated to be an efficient candidate for generating multiple quantum correlated beams by utilizing a phase-insensitive cascaded FWM (CFWM) process in a ^{85}Rb vapor cell [32–41].

With the rapid development of quantum technology, a high degree of quantum correlation is required to improve the communication fidelity of the quantum information protocol [3,9,42] and the measurement precision of quantum metrology [27,28,30,43,44]. Recently, our group theoretically [45] and experimentally [46] demonstrated that the bipartite quantum correlation generated from the phase-insensitive FWM process can be enhanced by introducing the phase-sensitive FWM process. Therefore, it is of great significance to study the possibility of enhancing the multipartite quantum correlation by introducing a phase-sensitive FWM process. In this paper, we propose a scheme for achieving the en-

*Corresponding author: ssliu@lps.ecnu.edu.cn

†Corresponding author: jtjing@phy.ecnu.edu.cn

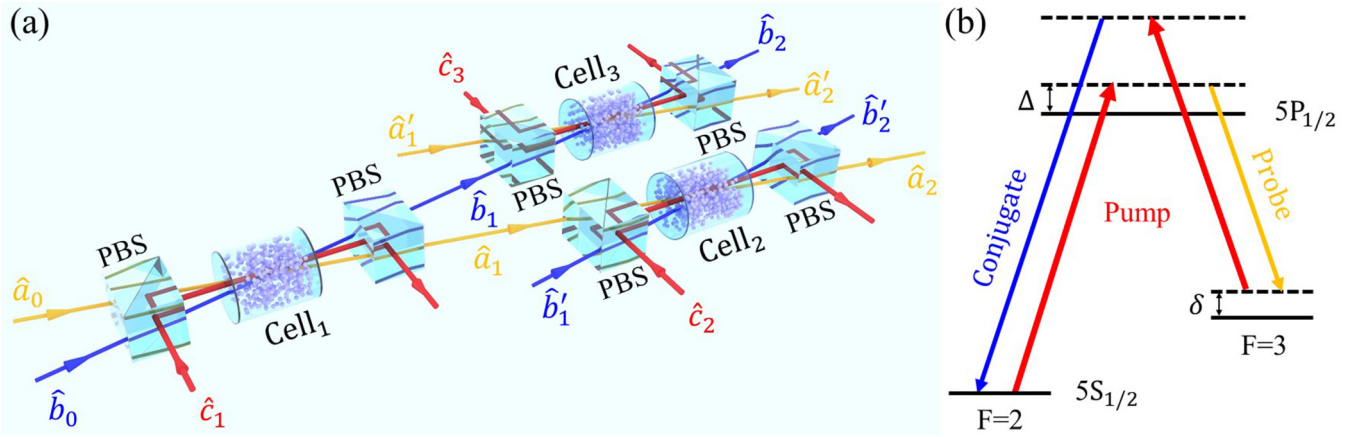

FIG. 1. The phase-sensitive CFWM process in a ^{85}Rb vapor cell for enhancing quadripartite quantum correlation. (a) Schematic view of the phase-sensitive CFWM process. PBS, polarizing beam splitter; cell$_1$, cell$_2$, and cell$_3$, ^{85}Rb vapor cells; $\hat{a}_0$ and $\hat{a}'_1$, coherent probe fields; $\hat{b}_0$ and $\hat{b}'_1$, coherent conjugate fields; $\hat{a}_1$ and $\hat{b}_1$, output fields of cell$_1$; $\hat{a}_2$, $\hat{b}'_2$, $\hat{a}'_2$, and $\hat{b}_2$, output fields of the phase-sensitive CFWM process; $\hat{c}_1$, $\hat{c}_2$, and $\hat{c}_3$, pump fields. All these field operators are annihilation operators associated with the corresponding optical fields. (b) Energy-level diagram of the double-Λ scheme in the D_1 line of ^{85}Rb for the single FWM process. Δ and δ stand for the one-photon detuning and two-photon detuning, respectively.

hancement of quadripartite quantum correlation based on a phase-sensitive CFWM process in a ^{85}Rb vapor cell. We show that the intensity-difference squeezing (IDS) among the four output beams produced by the phase-insensitive CFWM process [35,36] can be largely enhanced by introducing the phase-sensitive CFWM process. Actually, when the intensity gains of three FWM processes are equal, the IDS of the phase-sensitive CFWM process is at least 50% (3 dB) better than that of the corresponding phase-insensitive CFWM process if the intensity gain is greater than 1.16. For example, when the intensity gains of three FWM processes are all equal to 3, the IDS value of the phase-insensitive CFWM process is 0.040 (-13.979 dB), while the value of maximum IDS of the phase-sensitive CFWM process is 0.018 (-17.349 dB), which means that the IDS enhancement is about 55% (3.370 dB). We also show that the phase-sensitive CFWM process can be used to generate intensity-sum squeezing (ISS), which cannot be generated by the phase-insensitive CFWM process. Moreover, we show that the maximum squeezing value of IDS and the maximum squeezing value of ISS in our phase-sensitive CFWM process are equal. In addition, we investigate the effects of the losses and the phase fluctuations on the squeezing values of our phase-sensitive CFWM process and the corresponding phase-insensitive CFWM process with the same intensity gains. It is found that the squeezing enhancement of our phase-sensitive CFWM process holds also in the presence of the losses and the phase fluctuations.

The remainder of the paper is arranged as follows. In Sec. II, we briefly introduce the phase-sensitive CFWM process and derive expressions for the output fields produced by this cascaded system. The noise properties of the system are discussed in Sec. III. The IDS and the ISS among the four output beams generated from the current phase-sensitive CFWM process are also deduced in this section. In Sec. IV, the effects of the losses and the phase fluctuations on the squeezing values of our phase-sensitive CFWM process and the corresponding phase-insensitive CFWM process are discussed. Finally, a brief conclusion is given in Sec. V.

II. PHASE-SENSITIVE CFWM PROCESS

Our scheme for enhancing quadripartite quantum correlation is shown in Fig. 1. As shown in Fig. 1(a), two coherent fields, probe beam $\hat{a}_0$ and conjugate beam $\hat{b}_0$, are simultaneously and symmetrically crossed with a strong pump beam, $\hat{c}_1$, in the center of cell$_1$. Probe beam $\hat{a}_1$ and conjugate beam $\hat{b}_1$ are generated by the FWM process in cell$_1$. Then, probe beam $\hat{a}_1$ is sent into cell$_2$ with an additional phase θ_x, and conjugate beam $\hat{b}_1$ is sent into cell$_3$ with an additional phase θ_y simultaneously. θ_x and θ_y are caused by the distance between the two cells. Probe beam $\hat{a}_1 e^{i\theta_x}$ and coherent conjugate beam $\hat{b}'_1$ are simultaneously and symmetrically crossed with another strong pump beam, $\hat{c}_2$, in the center of cell$_2$. Meanwhile, conjugate beam $\hat{b}_1 e^{i\theta_y}$ and coherent probe beam $\hat{a}'_1$ are also crossed with a strong pump beam, $\hat{c}_3$, in the center of cell$_3$. Then, two probe beams, $\hat{a}_2$ and $\hat{a}'_2$, and two conjugate beams, $\hat{b}_2$ and $\hat{b}'_2$, are created via the FWM process in cell$_2$ and cell$_3$. These four output beams are quantum correlated. To ensure the phase matching of our scheme, carefully aligning the beams in three ^{85}Rb vapor cells (cell$_1$, cell$_2$, and cell$_3$) in turn is needed. First, by choosing a suitable lens combination, the two weak coherent beams (probe and conjugate beams $\hat{a}_0$ and $\hat{b}_0$) injected into cell$_1$ can be made to have almost the same waist in the center of cell$_1$. Second, by adjusting the injection angle of $\hat{a}_0$ and $\hat{b}_0$, the interference visibilities of the probe and conjugate output ports of cell$_1$ can be optimized to the maximum. In this way, the careful alignment of the beams in cell$_1$ can be completed. Then, the probe and conjugate beams output from cell$_1$ ($\hat{a}_1$ and $\hat{b}_1$) should be seeded into cell$_2$ and cell$_3$ by two $4f$ imaging systems, respectively. Meanwhile, the other input port of cell$_2$ (cell$_3$) should be seeded by another coherent beam $\hat{b}'_1$ ($\hat{a}'_1$). By the same token, the careful alignment of the beams in cell$_2$ and cell$_3$ can also be completed. Figure 1(b) depicts the energy-level diagram of a single FWM process in a ^{85}Rb vapor cell, where two pump photons can be converted to one probe photon and one conjugate photon. Since the pump beam is very strong in each single FWM

process, it can be regarded as a classical field. In this way, the interaction Hamiltonian of three FWM processes in the three cells mentioned above can be written as [47,48]

$$\hat{H}_1 = i\hbar\kappa_1 e^{i\theta_1}\hat{b}_1^{\dagger}\hat{a}_1^{\dagger} + \text{H.c.}, \tag{1}$$

$$\hat{H}_2 = i\hbar\kappa_2 e^{i\theta_2}\hat{b}_2'^{\dagger}\hat{a}_2^{\dagger} + \text{H.c.}, \tag{2}$$

$$\hat{H}_3 = i\hbar\kappa_3 e^{i\theta_3}\hat{b}_2^{\dagger}\hat{a}_2'^{\dagger} + \text{H.c.}, \tag{3}$$

where $\theta_j = 2\phi_{c_j}$ $(j = 1, 2, 3)$ and ϕ_{c_j} is the phase of the pump field $\hat{c}_j$. κ_j is the interaction strength of the FWM process in cell$_j$, which is not only dependent on the pump power but also dependent on one-photon detuning Δ and two-photon detuning δ. From Eqs. (1) to (3), the input-output relation of the phase-sensitive CFWM process can be written as

$$\begin{pmatrix} \hat{a}_2 \\ \hat{b}_2'^{\dagger} \\ \hat{a}_2' \\ \hat{b}_2^{\dagger} \end{pmatrix} = \begin{pmatrix} e^{i\theta_x}\sqrt{G_1G_2} & e^{i\theta_2}\sqrt{G_2-1} & 0 & e^{i(\theta_x+\theta_1)}\sqrt{(G_1-1)G_2} \\ e^{i(\theta_x-\theta_2)}\sqrt{G_1(G_2-1)} & \sqrt{G_2} & 0 & e^{i(\theta_x+\theta_1-\theta_2)}\sqrt{(G_1-1)(G_2-1)} \\ e^{i(\theta_3-\theta_1-\theta_y)}\sqrt{(G_1-1)(G_3-1)} & 0 & \sqrt{G_3} & e^{i(\theta_3-\theta_y)}\sqrt{G_1(G_3-1)} \\ e^{-i(\theta_1+\theta_y)}\sqrt{(G_1-1)G_3} & 0 & e^{-i\theta_3}\sqrt{G_3-1} & e^{-i\theta_y}\sqrt{G_1G_3} \end{pmatrix} \begin{pmatrix} \hat{a}_0 \\ \hat{b}_1'^{\dagger} \\ \hat{a}_1' \\ \hat{b}_0^{\dagger} \end{pmatrix}, \tag{4}$$

where $G_1 = \cosh^2(\kappa_1 t_1)$, $G_2 = \cosh^2(\kappa_2 t_2)$, and $G_3 = \cosh^2(\kappa_3 t_3)$, which are the intensity gains of three FWM processes. t_1, t_2, and t_3 are the mixing interaction times.

III. NOISE PROPERTIES OF THE SYSTEM

We start with the consideration of the IDS among the four output beams generated from the phase-sensitive CFWM process. Generally, the IDS among the quantum correlated beams generated by the CFWM process can be measured by utilizing the differential-measurement method. In the differential measurement, first, the probe beams ($\hat{a}_2$ and $\hat{a}_2'$) should be sent into one photodetector while the conjugate beams ($\hat{b}_2$ and $\hat{b}_2'$) are sent into the other photodetector. Then, the photocurrents of these two photodetectors should be subtracted by using a radio-frequency subtractor, which can give the noise power spectrum of the quantum correlated beams $\text{Var}(\hat{N}_{a_2} + \hat{N}_{a_2'} - \hat{N}_{b_2} - \hat{N}_{b_2'})_{\text{SQZ}}$. The corresponding shot-noise limit (SNL) of the quantum correlated beams can be obtained by using a coherent beam with a power equal to the total power of the quantum correlated beams. This coherent beam should be divided into two beams with a 50:50 beam splitter, and then the obtained two beams should be sent into two photodetectors to get the noise power of the differential photocurrent, which can give the level of the corresponding SNL, $\text{Var}(\hat{N}_{a_2} + \hat{N}_{a_2'} - \hat{N}_{b_2} - \hat{N}_{b_2'})_{\text{SNL}}$ [38]. In this way, the value of IDS among the four output beams with respect to the corresponding SNL can be given by

$$\begin{aligned} \text{IDS} &= \frac{\text{Var}(\hat{N}_{a_2} + \hat{N}_{a_2'} - \hat{N}_{b_2} - \hat{N}_{b_2'})_{\text{SQZ}}}{\text{Var}(\hat{N}_{a_2} + \hat{N}_{a_2'} - \hat{N}_{b_2} - \hat{N}_{b_2'})_{\text{SNL}}} \\ &= \frac{1 + \beta_1 + \beta_2 + \beta_3}{\gamma}, \end{aligned} \tag{5}$$

where $\gamma = G_1(2G_2 - 1) + (G_1 - 1)(2G_3 - 1) + [(G_1 - 1)(2G_2 - 1) + G_1(2G_3 - 1)]\beta_1 + (2G_2 - 1)\beta_2 + (2G_3 - 1)\beta_3 + 4[\sqrt{G_1(G_1-1)\beta_1}(-1 + G_2 + G_3)\cos(\psi_1) + \sqrt{(G_1-1)(G_2-1)G_2\beta_1\beta_2}\cos(\psi_1 - \psi_2) + \sqrt{G_1(G_2-1)G_2\beta_2}\cos(\psi_2) + \sqrt{(G_3-1)G_3(G_1-1)\beta_3}\cos(\psi_1 - \psi_3) + \sqrt{(G_3-1)G_3G_1\beta_1\beta_3}\cos(\psi_3)]$. β_1, β_2, and β_3 are the intensity ratios and are equal to $\langle\hat{N}_{b_0}\rangle/\langle\hat{N}_{a_0}\rangle$, $\langle\hat{N}_{b_1'}\rangle/\langle\hat{N}_{a_0}\rangle$, and $\langle\hat{N}_{a_1'}\rangle/\langle\hat{N}_{a_0}\rangle$, respectively. $\langle\hat{N}_{a_0}\rangle$ and $\langle\hat{N}_{b_0}\rangle$ represent the average input photon number of probe field $\hat{a}_0$ and conjugate field $\hat{b}_0$ sent into cell$_1$, respectively. $\langle\hat{N}_{b_1'}\rangle$ represents the average input photon number of conjugate field $\hat{b}_1'$ injected into cell$_2$, and $\langle\hat{N}_{a_1'}\rangle$ represents the average input photon number of probe field $\hat{a}_1'$ injected into cell$_3$. ψ_1 is equal to $\theta_1 - \theta_a - \theta_b$. ψ_2 is equal to $\theta_2 - \theta_a - \theta_{b1} - \theta_x$. ψ_3 is equal to $\theta_3 - \theta_{a1} - \theta_b - \theta_y$. θ_a and θ_{a1} and θ_b and θ_{b1} are the phases of the probe fields ($\hat{a}_0$ and $\hat{a}_1'$) and the conjugate fields ($\hat{b}_0$ and $\hat{b}_1'$), respectively. It is worth noting that $\text{Var}(\hat{N}_{a_2} + \hat{N}_{a_2'} - \hat{N}_{b_2} - \hat{N}_{b_2'})_{\text{SNL}}$ is just the sum of the average photon number of the four output beams (a_2, a_2', b_2, and b_2'). When $\beta_1 = \beta_2 = \beta_3 = 0$, the value of IDS among the four output beams is given by $1/[1 - 2G_3 + 2G_1(-1 + G_2 + G_3)]$, which agrees well with the result of the phase-insensitive CFWM process shown in Refs. [35,36]. Compared with the IDS of the phase-insensitive CFWM process, the IDS of the phase-sensitive CFWM process as indicated by Eq. (5) has some phase-sensitive factors, which will bring the possibility of IDS enhancement. Moreover, it can be seen from Eq. (5) that the IDS enhancement is dependent not only on the intensity gains (G_1, G_2, and G_3) but also on the intensity ratios (β_1, β_2, and β_3) and the phases (ψ_1, ψ_2, and ψ_3) of the input beams in the phase-sensitive CFWM process. Therefore, it is valuable to study how these parameters influence the performance of the phase-sensitive CFWM process.

First, in order to analyze the effect of the intensity gain on the IDS enhancement of the phase-sensitive CFWM process, we plot the IDS values of the phase-sensitive CFWM process (the phase-insensitive CFWM process) as a function of the intensity gains G_2 and G_3 when $\psi_1 = \psi_2 = \psi_3 = 0$ and $\beta_1 = \beta_2 = \beta_3 = 1$ ($\beta_1 = \beta_2 = \beta_3 = 0$) for gains G_1 of 2, 3, and 4, as shown in Fig. 2. It can be seen that the IDS values of both the phase-insensitive CFWM process and the phase-sensitive CFWM process decrease with the increase of gains G_1, G_2, and G_3. Moreover, the IDS of the phase-sensitive CFWM process is always better than that of the phase-insensitive CFWM process, clearly showing the squeezing enhancement. In the current situation, for gains G_1 of 2, 3, and 4, the IDS of the phase-sensitive CFWM process is enhanced by about 48% (2.833 dB), 41% (2.320 dB), and 35% (1.871 dB) compared to that of the phase-insensitive CFWM process when $G_2 = G_3 = 4$, respectively.

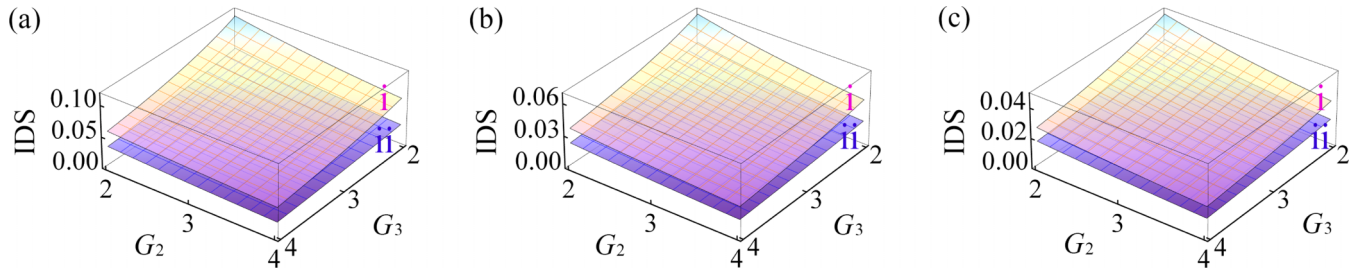

FIG. 2. The values of IDS as a function of G_2 and G_3 for different values of G_1. Curved surface i represents the squeezing value of the phase-insensitive CFWM process, and curved surface ii represents the squeezing value of the phase-sensitive CFWM process under the condition of $\psi_1 = \psi_2 = \psi_3 = 0$ and $\beta_1 = \beta_2 = \beta_3 = 1$. (a) $G_1 = 2$. (b) $G_1 = 3$. (c) $G_1 = 4$.

Second, we investigate how the IDS enhancement of the phase-sensitive CFWM process depends on the intensity ratio. In order to study this effect, we plot the IDS values (plane i for the phase-insensitive CFWM process and curved surface ii for the phase-sensitive CFWM process) as a function of ratios β_2 and β_3 by keeping the gains $G_1 = G_2 = G_3 = 3$ and the phases $\psi_1 = \psi_2 = \psi_3 = 0$ for different ratios β_1, as shown in Fig. 3. As we can see, when ratios β_2 and β_3 are the particular values given in the caption, the maximum squeezing value of the phase-sensitive CFWM process for ratios β_1 of 0, 0.5, 1, and 5 can be obtained, which are 0.034 (−14.747 dB), 0.019 (−17.236 dB), 0.018 (−17.349 dB), and 0.021 (−16.819 dB), respectively. With the same gains $G_1 = G_2 = G_3 = 3$, the IDS value of the phase-insensitive CFWM process is 0.040 (−13.979 dB). In other words, an IDS enhancement of nearly 55% (3.370 dB) can be achieved in our phase-sensitive CFWM process compared to the phase-insensitive CFWM process with the same gains $G_1 = G_2 = G_3 = 3$ [35,36] when $\beta_1 = 1$ and $\beta_2 = \beta_3 = 0.0977$. In addition, in the situation with $G_1 = G_2 = G_3 = 3$, the IDS value of our current scheme [0.018 (−17.349 dB)] is about 10% (0.447 dB) better than that of the previous scheme with the same intensity gains [0.020 (−16.902 dB)] presented in Ref. [49], which clearly shows the novelty and the advantage of our proposed technique in enhancing the quantum correlation.

Third, in order to explore how the phase influences the IDS enhancement of the phase-sensitive CFWM process, we fix the gains $G_1 = G_2 = G_3 = 3$ and the ratios $\beta_1 = 1$ and $\beta_2 = \beta_3 = 0.0977$ and plot the IDS values (plane i for the phase-insensitive CFWM process and curved surface ii for the phase-sensitive CFWM process) as a function of ψ_2 and ψ_3 for different phases ψ_1, as shown in Fig. 4. It can be seen that for a given ψ_1, the maximum squeezing value of the phase-sensitive CFWM process can be achieved when

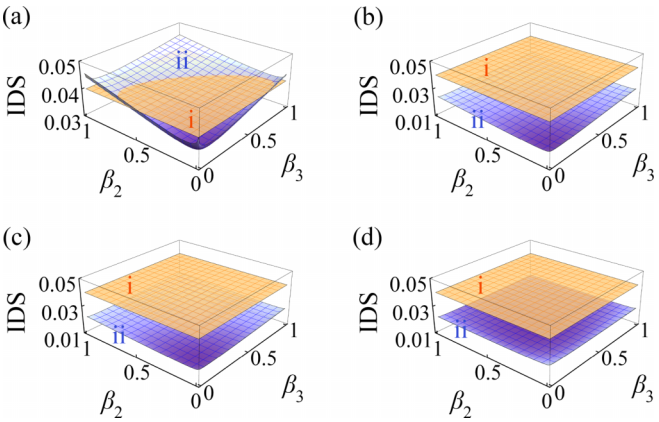

FIG. 3. The values of IDS as a function of the ratios β_2 and β_3 for different values of β_1 when $\psi_1 = \psi_2 = \psi_3 = 0$ and $G_1 = G_2 = G_3 = 3$. Plane i represents the squeezing value of the phase-insensitive CFWM process, and curved surface ii represents the squeezing value of the phase-sensitive CFWM process. (a) $\beta_1 = 0$: the maximum squeezing value of the phase-sensitive CFWM process is achieved when $\beta_2 = 0.1168$ and $\beta_3 = 0.0778$. (b) $\beta_1 = 0.5$: the maximum squeezing value of the phase-sensitive CFWM process is achieved when $\beta_2 = 0.078$ and $\beta_3 = 0.0728$. (c) $\beta_1 = 1$: the maximum squeezing value of the phase-sensitive CFWM process is achieved when $\beta_2 = \beta_3 = 0.0977$. (d) $\beta_1 = 5$: the maximum squeezing value of the phase-sensitive CFWM process is achieved when $\beta_2 = 0.3098$ and $\beta_3 = 0.3615$.

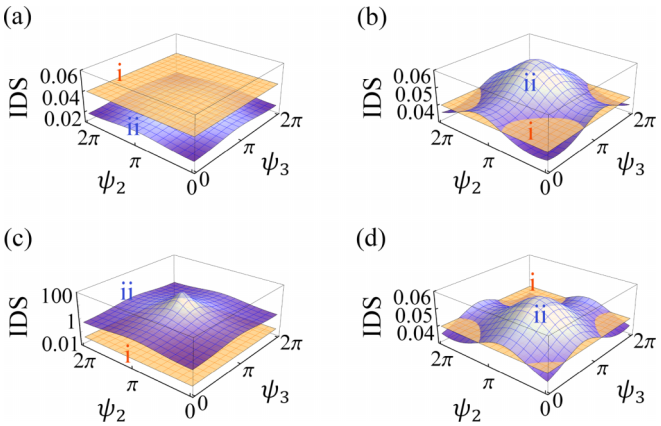

FIG. 4. The values of IDS as a function of phases ψ_2 and ψ_3 for different values of ψ_1 when $G_1 = G_2 = G_3 = 3$, $\beta_1 = 1$, and $\beta_2 = \beta_3 = 0.0977$. Plane i represents the squeezing value of the phase-insensitive CFWM process, and curved surface ii represents the squeezing value of the phase-sensitive CFWM process. (a) $\psi_1 = 0$: the maximum squeezing value of the phase-sensitive CFWM process is achieved when $\psi_2 = \psi_3 = 0, 2\pi$. (b) $\psi_1 = \pi/2$: the maximum squeezing value of the phase-sensitive CFWM process is achieved when $\psi_2 = \psi_3 = 0.2181\pi$. (c) $\psi_1 = \pi$: the maximum squeezing value of the phase-sensitive CFWM process is achieved when $\psi_2 = \psi_3 = 0, 2\pi$. (d) $\psi_1 = 3\pi/2$: the maximum squeezing value of the phase-sensitive CFWM process is achieved when $\psi_2 = \psi_3 = 1.783\pi$.

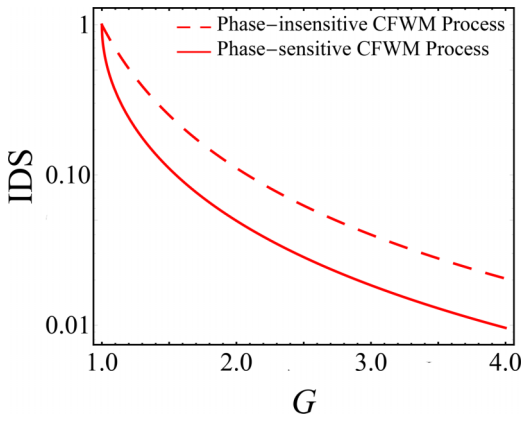

FIG. 5. The values of IDS as a function of the intensity gain G. Red dashed line: the squeezing value of the phase-insensitive CFWM process; red solid line: the maximum squeezing value of the phase-sensitive CFWM process as predicted by Eq. (6).

phases ψ_2 and ψ_3 are the values given in the caption. In the current situation, the maximum squeezing value of the phase-sensitive CFWM process for phases ψ_1 of 0, $\pi/2$, π, and $3\pi/2$ are 0.018 (−17.349 dB), 0.034 (−14.692 dB), 0.558 (−2.533 dB), and 0.034 (−14.692 dB), respectively. It can also be found that the squeezing value of the phase-insensitive CFWM process is always 0.040 (−13.979 dB). Therefore, compared to the phase-insensitive CFWM process with the same gains $G_1 = G_2 = G_3 = 3$ [35,36], our phase-sensitive CFWM process can lead to about a 55% (3.370 dB) IDS enhancement when $\psi_1 = \psi_2 = \psi_3 = 0, 2\pi$.

Fourth, we consider the more general situation of the IDS of our phase-sensitive CFWM process, in which the intensity gains $G_1 = G_2 = G_3 = G$ ($1 \leqslant G \leqslant 4$). Based on the experimental results in our previous work [35], this intensity gain range requires each pump beam in our scheme to have a power of about 0 to 240 mW. Here one can easily calculate the maximum squeezing value of IDS from Eq. (5), which is given by

$$\mathrm{IDS}_{\max} = \frac{1 + 4G^2 - (2G-1)\sqrt{4G^2+1}}{\zeta}, \tag{6}$$

where $\zeta = -1 + 6G - 16G^2 + 16G^3 + 4\sqrt{G-1}G^{\frac{3}{2}}(2G-1) - \sqrt{4G^2+1}(2G-1)^2 + 4\sqrt{2(G-1)}G^{\frac{3}{2}}\sqrt{4G + (\sqrt{4G^2+1}+1)(-2+\frac{1}{G})(\sqrt{G-1}+\sqrt{G})}$. This value can be achieved when $\beta_1 = 1$, $\beta_2 = \beta_3 = \frac{-1+3G-6G^2+4G^3-(1-3G+2G^2)\sqrt{4G^2+1}}{2G(G-1)}$, and $\psi_1 = \psi_2 = \psi_3 = 0, 2\pi$. It is interesting to examine how the IDS enhancement varies with the intensity gain G. These results are summarized in Fig. 5. It can be found that the squeezing values of these two configurations decrease with the increase of the intensity gain. Moreover, the maximum squeezing value of the phase-sensitive CFWM process is always better (lower) than the squeezing value of the phase-insensitive CFWM process. In the current case with $G_1 = G_2 = G_3 = G$, the IDS value of the phase-insensitive CFWM process is at least two times that of the phase-sensitive CFWM process if $G \geqslant 1.16$. In other words, the IDS of the phase-sensitive CFWM process is at least 50% (3 dB) better than that of the phase-insensitive CFWM process if $G_1 = G_2 = G_3 \geqslant 1.16$.

We now consider the ISS generated from the phase-sensitive CFWM process. The value of ISS among the four output beams of our phase-sensitive cascaded scheme with respect to the SNL is given by

$$\mathrm{ISS} = \frac{\mathrm{Var}(\hat{N}_{a_2} + \hat{N}_{a_2'} + \hat{N}_{b_2} + \hat{N}_{b_2'})_{\mathrm{SQZ}}}{\mathrm{Var}(\hat{N}_{a_2} + \hat{N}_{a_2'} + \hat{N}_{b_2} + \hat{N}_{b_2'})_{\mathrm{SNL}}} = \frac{1 + \beta_1 + \beta_2 + \beta_3 + \xi}{\gamma}, \tag{7}$$

where $\xi = 8G_1[G_1(-1+G_2+G_3)^2(1+\beta_1) + G_2^2(-\beta_1+\beta_2) - G_2(-1-2\beta_1+2G_3+2G_3\beta_1+\beta_2) + (-1+G_3)(1+\beta_1-G_3+G_3\beta_3)] + 8\sqrt{G_1(G_1-1)\beta_1}[-1+G_2+G_3-2G_2G_3+2G_1(-1+G_2+G_3)^2]\cos(\psi_1) + 16G_1(-1+G_2+G_3)\sqrt{(G_1-1)G_2(G_2-1)\beta_1\beta_2}\cos(\psi_1-\psi_2) + 8\sqrt{G_1G_2(G_2-1)\beta_2}[1-2G_3+2G_1(-1+G_2+G_3)]\cos(\psi_2) + 16G_1(-1+G_2+G_3)\sqrt{(G_1-1)G_3(G_3-1)\beta_3}\cos(\psi_1-\psi_3) + 16\sqrt{G_1(G_1-1)G_2(G_2-1)G_3(G_3-1)\beta_2\beta_3}\cos(\psi_1-\psi_2-\psi_3) + 8\sqrt{G_1G_3(G_3-1)\beta_1\beta_3}[1-2G_2+2G_1(-1+G_2+G_3)]\cos(\psi_3)$. This result can easily be calculated through the use of Eq. (4). As we can see from Eq. (7), the ISS value of the phase-sensitive CFWM process also changes with G_1, G_2, G_3, β_1, β_2, β_3, ψ_1, ψ_2, and ψ_3. Therefore, it is also necessary to explore how these parameters influence the ISS properties of the phase-sensitive CFWM process. For simplicity, we set all intensity gains of each FWM process to be equal, and we use G to denote the intensity gain, i.e., $G_1 = G_2 = G_3 = G$. In Fig. 6, we plot the ISS values of the phase-sensitive CFWM process as a function of the intensity ratios β_2 and β_3 when the phases $\psi_1 = \psi_2 = \psi_3 = \pi$ for ratios β_1 of 0, 0.5, 1, and 5 and gains G of 2, 3, and 4. It is clear that in the case of $\beta_1 = 1$, the maximum squeezing values of ISS for different gains can be achieved when the intensity ratios β_2 and β_3 are the values given in the caption of Fig. 6, which are 0.049 (−13.054 dB), 0.018 (−17.349 dB), and 0.010 (−20.177 dB) for gains G of 2, 3, and 4 respectively. In addition, as shown in Figs. 6(a), 6(e), and 6(i), the ISS values for different intensity gains are higher than the SNL (ISS = 1) when β_2 and β_3 are equal to zero, which means that the phase-insensitive CFWM process cannot generate the ISS. As shown in Fig. 7, we plot the ISS values of the phase-sensitive CFWM process as a function of phases ψ_2 and ψ_3 for different values of intensity gain G and phase ψ_1 when the intensity ratios β_1, β_2, and β_3 are particular values. It can be seen that when the phases $\psi_1 = \psi_2 = \psi_3 = \pi$, the maximum squeezing values of ISS for different gains can be achieved, which are 0.049 (−13.054 dB), 0.018 (−17.349 dB), and 0.010 (−20.177 dB) for gains G of 2, 3, and 4 respectively. Furthermore, we can find from Figs. 6 and 7 that the ISS value decreases with the increase of the intensity gain.

Similarly, we consider the maximum squeezing value of ISS of our phase-sensitive CFWM process in the general case of $G_1 = G_2 = G_3 = G$ ($1 \leqslant G \leqslant 4$), which can easily be calculated from Eq. (7). It is expressed as

$$\mathrm{ISS}_{\max} = \frac{1 + 4G^2 - (2G-1)\sqrt{4G^2+1}}{\zeta}. \tag{8}$$

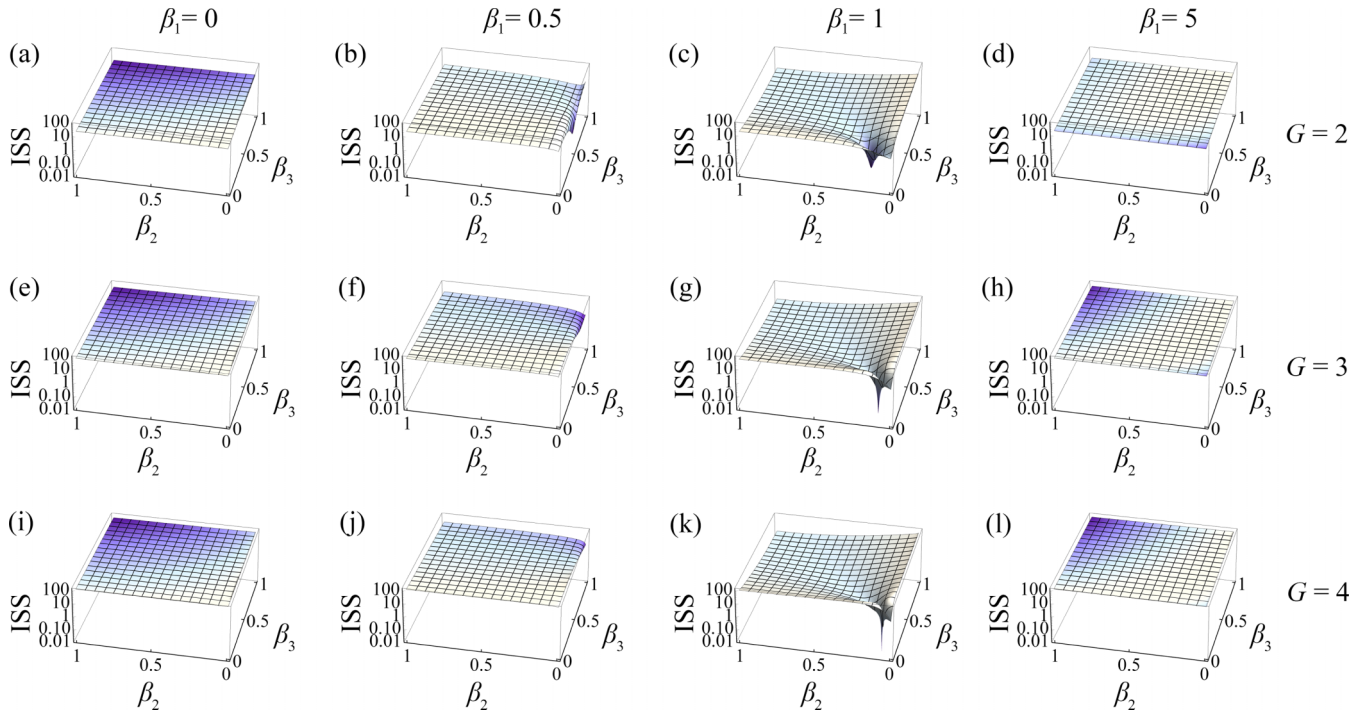

FIG. 6. The ISS values of the phase-sensitive CFWM process as a function of β_2 and β_3 when $\psi_1 = \psi_2 = \psi_3 = \pi$ for ratios β_1 of 0, 0.5, 1, and 5 and gains G of 2, 3, and 4. (a)–(d) $G = 2$: the maximum squeezing value is achieved when $\beta_1 = 1$ and $\beta_2 = \beta_3 = 0.1577$. (e),–(h) $G = 3$: the maximum squeezing value is achieved when $\beta_1 = 1$ and $\beta_2 = \beta_3 = 0.0977$. (i)–(l) $G = 4$: the maximum squeezing value is achieved when $\beta_1 = 1$ and $\beta_2 = \beta_3 = 0.0705$.

This value is achieved when $\beta_1 = 1$, $\beta_2 = \beta_3 = \frac{-1+3G-6G^2+4G^3-(1-3G+2G^2)\sqrt{4G^2+1}}{2G(G-1)}$, and $\psi_1 = \psi_2 = \psi_3 = \pi$. From Eqs. (6) and (8), it is clear that the values of the maximum IDS and the maximum ISS are equal.

IV. EFFECTS OF THE LOSSES AND THE PHASE FLUCTUATIONS

Since there are unavoidable losses and phase fluctuations in the real experiment, in this section, we study the effects of the losses and the phase fluctuations on the squeezing values

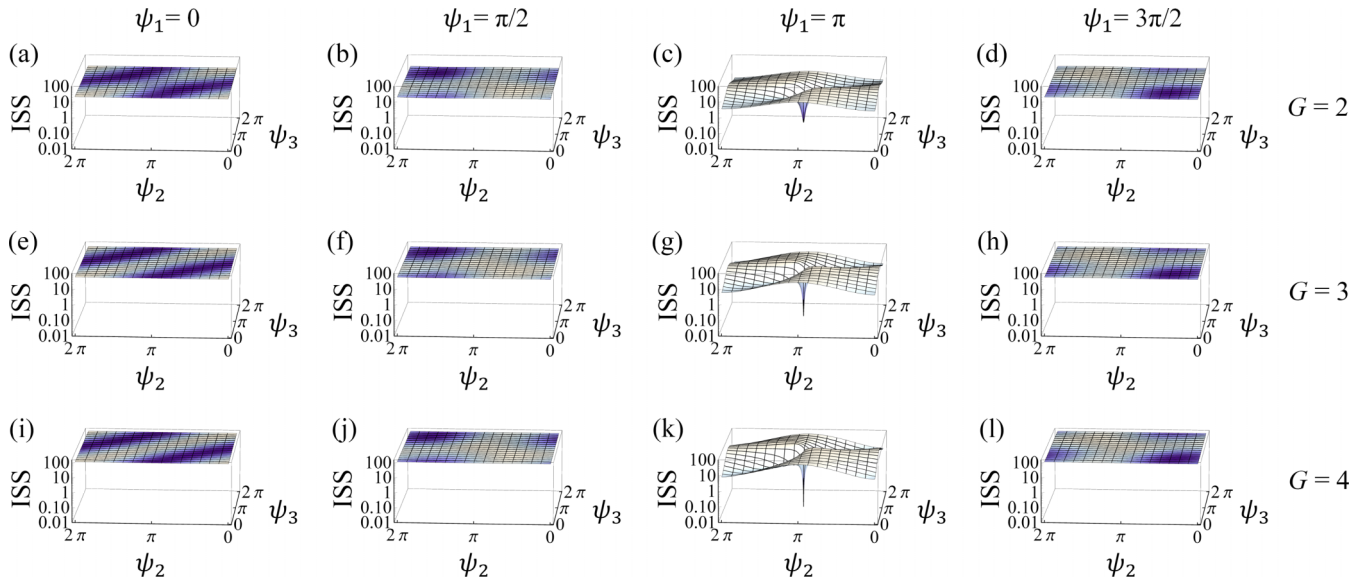

FIG. 7. The ISS values of the phase-sensitive CFWM process as a function of ψ_2 and ψ_3 when β_1, β_2, and β_3 are certain values for phases ψ_1 of 0, $\pi/2$, π, and $3\pi/2$ and gains G of 2, 3, and 4. (a)–(d) $G = 2$, $\beta_1 = 1$, and $\beta_2 = \beta_3 = 0.1577$. (e)–(h) $G = 3$, $\beta_1 = 1$, and $\beta_2 = \beta_3 = 0.0977$. (i)–(l) $G = 4$, $\beta_1 = 1$, and $\beta_2 = \beta_3 = 0.0705$. All of the maximum squeezing values for different gains are achieved when $\psi_1 = \psi_2 = \psi_3 = \pi$.

of our phase-sensitive CFWM process and the corresponding phase-insensitive CFWM process with the same intensity gains. The discussion is divided into two parts: the effect of the losses is investigated in Sec. IV A, while Sec. IV B concerns the effect of the phase fluctuations.

A. Effect of the losses

We first study the effect of the losses in the case of ideal phase locking (no phase fluctuations). By modeling the losses with the optical beam splitters [50–52], the output fields of the three FWM processes in our scheme can be written as

$$\begin{aligned}
\hat{a}_{1,\mathrm{loss}} =&\sqrt{(1-\eta_1)(1-\tau)}(\sqrt{1-L_1}\hat{a}_1+\sqrt{L_1}\hat{v}_1)\\
&+\sqrt{1-(1-\eta_1)(1-\tau)}\hat{v}_2,\\
\hat{b}_{1,\mathrm{loss}} =&\sqrt{1-\eta_2}(\sqrt{1-L_2}\hat{b}_1+\sqrt{L_2}\hat{v}_3)\\
&+\sqrt{\eta_2}\hat{v}_4,\\
\hat{a}_{2,\mathrm{loss}} =&\sqrt{(1-\eta_3)(1-\lambda_1)}(\sqrt{1-L_3}\hat{A}_2+\sqrt{L_3}\hat{v}_5)\\
&+\sqrt{1-(1-\eta_3)(1-\lambda_1)}\hat{v}_6,\\
\hat{b}'_{2,\mathrm{loss}} =&\sqrt{(1-\eta_4)(1-\lambda_2)}(\sqrt{1-L_4}\hat{B}'_2\\
&+\sqrt{L_4}\hat{v}_7)+\sqrt{1-(1-\eta_4)(1-\lambda_2)}\hat{v}_8,\\
\hat{a}'_{2,\mathrm{loss}} =&\sqrt{(1-\eta_5)(1-\lambda_3)}(\sqrt{1-L_5}\hat{A}'_2\\
&+\sqrt{L_5}\hat{v}_9)+\sqrt{1-(1-\eta_5)(1-\lambda_3)}\hat{v}_{10},\\
\hat{b}_{2,\mathrm{loss}} =&\sqrt{(1-\eta_6)(1-\lambda_4)}(\sqrt{1-L_6}\hat{B}_2+\sqrt{L_6}\hat{v}_{11})\\
&+\sqrt{1-(1-\eta_6)(1-\lambda_4)}\hat{v}_{12},
\end{aligned}\tag{9}$$

where $\hat{A}_2=\sqrt{G_2}\hat{a}_{1,\mathrm{loss}}e^{i\theta_x}+e^{i\theta_2}\sqrt{G_2-1}\hat{b}_1'^{\dagger}$, $\hat{B}'_2=\sqrt{G_2}\hat{b}'_1+e^{i\theta_2}\sqrt{G_2-1}\hat{a}^{\dagger}_{1,\mathrm{loss}}e^{-i\theta_x}$, $\hat{A}'_2=\sqrt{G_3}\hat{a}'_1+e^{i\theta_3}\sqrt{G_3-1}\hat{b}^{\dagger}_{1,\mathrm{loss}}e^{-i\theta_y}$, and $\hat{B}_2=\sqrt{G_3}\hat{b}_{1,\mathrm{loss}}e^{i\theta_y}+e^{i\theta_3}\sqrt{G_3-1}\hat{a}_1'^{\dagger}$. L_1, L_2, L_3, L_4, L_5, and L_6 are the absorption losses of $\hat{a}_1$, $\hat{b}_1$, $\hat{a}_2$, $\hat{b}'_2$, $\hat{a}'_2$, and $\hat{b}_2$ in three ^{85}Rb vapor cells, respectively. η_1, η_2, η_3, η_4, η_5, and η_6 are the propagation losses of $\hat{a}_1$, $\hat{b}_1$, $\hat{a}_2$, $\hat{b}'_2$, $\hat{a}'_2$, and $\hat{b}_2$ due to imperfect propagation, respectively. λ_1, λ_2, λ_3, and λ_4 represent the detection losses of $\hat{a}_2$, $\hat{b}'_2$, $\hat{a}'_2$, and $\hat{b}_2$ due to imperfect quantum efficiencies of the detectors, respectively. τ is the extraction loss introduced by extracting the interference signal from beam $\hat{a}_1$ for phase locking [53]. $\hat{v}_i$ $(i=1,2,\ldots,12)$ represents the vacuum field introduced by losses. For simplicity, we consider all the absorption losses (L_1, L_2, L_3, L_4, L_5, and L_6) as L, all the propagation losses (η_1, η_2, η_3, η_4, η_5, and η_6) as η, and all the detection losses (λ_1, λ_2, λ_3, and λ_4) as λ. In general, the measurements can be performed by using silicon photodetectors (PDB450, Thorlabs) with a transimpedance gain of 10^5 V/A and quantum efficiency of about 97%, i.e., $\lambda=0.03$. In this way, when considering losses in experiment ($L=0.05$, $\eta=0.03$, $\lambda=0.03$, $\tau=0.01$), we can calculate the maximum squeezing value of the phase-sensitive CFWM process and the squeezing value of the corresponding phase-insensitive CFWM process with the same intensity gains $G_1=G_2=G_3=G$. As shown in Fig. 8, the solid and dashed lines stand for the maximum squeezing value of the phase-sensitive CFWM process and the squeezing value of the phase-insensitive CFWM process in the lossy situation, respectively. We can see that the squeezing values of both the phase-sensitive CFWM process and the phase-insensitive CFWM process decrease with the increase of the intensity gain G. Moreover, we find that the squeezing value of the phase-sensitive CFWM process is always better (lower) than that of the phase-insensitive CFWM process, demonstrating that the enhancement of our technique holds also in the presence of the losses.

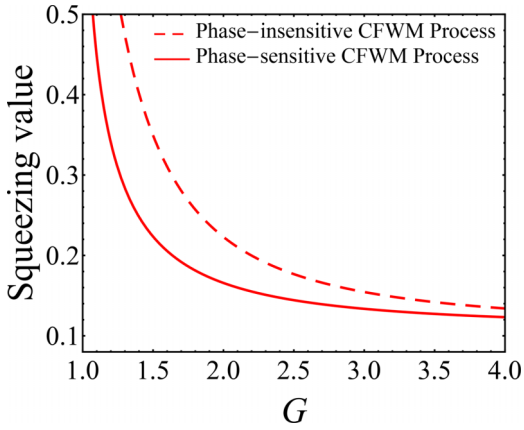

FIG. 8. Comparison of squeezing values between the phase-sensitive CFWM process and the corresponding phase-insensitive CFWM process with the same intensity gain G in the lossy situation of $L=0.05$, $\eta=0.03$, $\lambda=0.03$, $\tau=0.01$. Solid line: the maximum squeezing value of the phase-sensitive CFWM process; dashed line: the squeezing value of the phase-insensitive CFWM process.

B. Effect of the phase fluctuations

In our scheme, since three phase locking processes [54–60] are needed, the achieved squeezing value is undoubtedly affected by the quality of these three phase-locking processes. Therefore, in order to ensure the feasibility of our proposal, we study the effect of the phase fluctuations on the squeezing value of our phase-sensitive CFWM process by introducing three phase deviations. In this way, fields $\hat{a}_1$, $\hat{b}_1$, $\hat{A}_2$, $\hat{B}'_2$, $\hat{A}'_2$, and $\hat{B}_2$ in Eq. (9) can be rewritten as

$$\begin{aligned}
\hat{a}_1 &= \sqrt{G_1}\hat{a}_0e^{i\delta\theta_1}+e^{i\theta_1}\sqrt{G_1-1}\hat{b}_0^{\dagger},\\
\hat{b}_1 &= \sqrt{G_1}\hat{b}_0+e^{i\theta_1}\sqrt{G_1-1}\hat{a}_0^{\dagger}e^{-i\delta\theta_1},\\
\hat{A}_2 &= \sqrt{G_2}\hat{a}_{1,\mathrm{loss}}e^{i\theta_x}e^{i\delta\theta_2}+e^{i\theta_2}\sqrt{G_2-1}\hat{b}_1'^{\dagger},\\
\hat{B}'_2 &= \sqrt{G_2}\hat{b}'_1+e^{i\theta_2}\sqrt{G_2-1}\hat{a}^{\dagger}_{1,\mathrm{loss}}e^{-i\theta_x}e^{-i\delta\theta_2},\\
\hat{A}'_2 &= \sqrt{G_3}\hat{a}'_1+e^{i\theta_3}\sqrt{G_3-1}\hat{b}^{\dagger}_{1,\mathrm{loss}}e^{-i\theta_y}e^{-i\delta\theta_3},\\
\hat{B}_2 &= \sqrt{G_3}\hat{b}_{1,\mathrm{loss}}e^{i\theta_y}e^{i\delta\theta_3}+e^{i\theta_3}\sqrt{G_3-1}\hat{a}_1'^{\dagger},
\end{aligned}\tag{10}$$

where $\delta\theta_1$, $\delta\theta_2$, and $\delta\theta_3$ are the phase deviations of the three phase-locking processes. For simplicity, we consider all the phase deviations to be independent and equal, and we use $\delta\theta$ to denote the phase deviation, i.e., $\delta\theta=\delta\theta_1=\delta\theta_2=\delta\theta_3$. Based on Eqs. (9) and (10), we can calculate the maximum squeezing value of our phase-sensitive CFWM process and the squeezing value of the corresponding phase-insensitive CFWM process with the same intensity gains $G_1=G_2=G_3=G$. As shown in Fig. 9, when considering intensity gain and losses in experiment ($G=3$, $L=0.05$, $\eta=0.03$, $\lambda=$

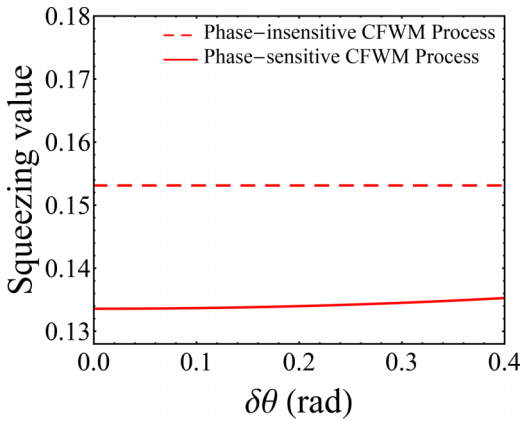

FIG. 9. The squeezing values as a function of the phase fluctuation $\delta\theta$ when $G = 3$, $L = 0.05$, $\eta = 0.03$, $\lambda = 0.03$, and $\tau = 0.01$. Solid line: the maximum squeezing value of the phase-sensitive CFWM process; dashed line: the squeezing value of the corresponding phase-insensitive CFWM process.

0.03, $\tau = 0.01$), we plot the maximum squeezing value of our phase-sensitive CFWM process and the squeezing value of the corresponding phase-insensitive CFWM process as a function of the phase fluctuation $\delta\theta$. It can be found that the maximum squeezing value of the phase-sensitive CFWM process (solid line) is always better (lower) than the squeezing value of the corresponding phase-insensitive CFWM process (dashed line) for $\delta\theta \leqslant 0.4$ rad, which indicates that the squeezing enhancement of our phase-sensitive CFWM process holds also in the presence of the losses and the phase fluctuations. In fact, the phase fluctuations of our scheme can be much less than 0.4 rad, enabled by the phase-locking technology based on a micro control unit [46]. In this sense, this proposal is feasible.

V. CONCLUSION

In conclusion, we have theoretically studied a scheme for enhancing the quadripartite quantum correlation via a phase-sensitive CFWM process in a ^{85}Rb vapor cell. We found that the IDS among the four output beams generated from the phase-insensitive CFWM process [35,36] can be largely enhanced by introducing a phase-sensitive CFWM process. Moreover, we found that our phase-sensitive CFWM process can generate the ISS, which can never be realized by the phase-insensitive CFWM process. Interestingly, we found that the maximum squeezing values of these two types of squeezing in our phase-sensitive CFWM process are the same when the intensity gains of the three FWM processes are equal. In addition, we explored the effects of the losses and the phase fluctuations on the squeezing values of our phase-sensitive CFWM process and the corresponding phase-insensitive CFWM process with the same intensity gains. We found that the squeezing enhancement of our phase-sensitive CFWM process holds also in the presence of the losses and the phase fluctuations, which ensures the feasibility of our scheme. These findings pave the way for experimental implementation and may have applications in quantum metrology and quantum communication.

ACKNOWLEDGMENTS

This work was funded by the Innovation Program of Shanghai Municipal Education Commission (Grant No. 2021-01-07-00-08-E00100), the Program of Shanghai Academic Research Leader (Grant No. 22XD1400700), the National Natural Science Foundation of China (Grants No. 11874155, No. 91436211, No. 11374104, and No. 12174110), the Basic Research Project of Shanghai Science and Technology Commission (Grant No. 20JC1416100), the Natural Science Foundation of Shanghai (Grant No. 17ZR1442900), the Minhang Leading Talents (Grant No. 201971), the Shanghai Sailing Program (Grant No. 21YF1410800), the Natural Science Foundation of Chongqing, China (Grant No. CSTB2022NSCQ-MSX0893), the Shanghai Municipal Science and Technology Major Project, (Grant No. 2019SHZDZX01), and the 111 project (Grant No. B12024).

[1] A. Einstein, B. Podolsky, and N. Rosen, Phys. Rev. **47**, 777 (1935).
[2] D. M. Greenberger, M. A. Horne, and A. Zeilinger, Phys. Today **46**(8), 22 (1993).
[3] S. L. Braunstein and P. van Loock, Rev. Mod. Phys. **77**, 513 (2005).
[4] H. J. Kimble, Nature (London) **453**, 1023 (2008).
[5] N. C. Menicucci, P. van Loock, M. Gu, C. Weedbrook, T. C. Ralph, and M. A. Nielsen, Phys. Rev. Lett. **97**, 110501 (2006).
[6] P. van Loock and S. L. Braunstein, Phys. Rev. Lett. **84**, 3482 (2000).
[7] J. Jing, J. Zhang, Y. Yan, F. Zhao, C. Xie, and K. Peng, Phys. Rev. Lett. **90**, 167903 (2003).
[8] T. Aoki, N. Takei, H. Yonezawa, K. Wakui, T. Hiraoka, A. Furusawa, and P. van Loock, Phys. Rev. Lett. **91**, 080404 (2003).
[9] H. Yonezawa, T. Aoki, and A. Furusawa, Nature (London) **431**, 430 (2004).
[10] S. Armstrong, J. F. Morizur, J. Janousek, B. Hage, N. Treps, P. K. Lam, and H. A. Bachor, Nat. Commun. **3**, 1026 (2012).
[11] M. Pysher, Y. Miwa, R. Shahrokhshahi, R. Bloomer, and O. Pfister, Phys. Rev. Lett. **107**, 030505 (2011).
[12] O. Pinel, P. Jian, R. M. de Araújo, J. Feng, B. Chalopin, C. Fabre, and N. Treps, Phys. Rev. Lett. **108**, 083601 (2012).
[13] S. Yokoyama, R. Ukai, S. C. Armstrong, C. Sornphiphatphong, T. Kaji, S. Suzuki, J-I. Yoshikawa, H. Yonezawa, N. C. Menicucci, and A. Furusawa, Nat. Photonics **7**, 982 (2013).
[14] W. Asavanant, Y. Shiozawa, S. Yokoyama, B. Charoensombutamon, H. Emura, R. N. Alexander, S. Takeda, J.-I. Yoshikawa, N. C. Menicucci, H. Yonezawa, and A. Furusawa, Science **366**, 373 (2019).

[15] M. V. Larsen, X. Guo, C. R. Breum, J. S. Neergaard-Nielsen, and U. L. Andersen, Science **366**, 369 (2019).
[16] M. Chen, N. C. Menicucci, and O. Pfister, Phys. Rev. Lett. **112**, 120505 (2014).
[17] J. Roslund, R. M. de Araújo, S. Jiang, C. Fabre, and N. Treps, Nat. Photonics **8**, 109 (2014).
[18] C. F. McCormick, V. Boyer, E. Arimondo, and P. D. Lett, Opt. Lett. **32**, 178 (2007).
[19] V. Boyer, A. M. Marino, R. C. Pooser, and P. D. Lett, Science **321**, 544 (2008).
[20] C. S. Embrey, M. T. Turnbull, P. G. Petrov, and V. Boyer, Phys. Rev. X **5**, 031004 (2015).
[21] B. J. Lawrie, P. G. Evans, and R. C. Pooser, Phys. Rev. Lett. **110**, 156802 (2013).
[22] B. J. Lawrie and R. C. Pooser, Opt. Express **21**, 7549 (2013).
[23] A. M. Marino, V. Boyer, R. C. Pooser, P. D. Lett, K. Lemons, and K. M. Jones, Phys. Rev. Lett. **101**, 093602 (2008).
[24] A. M. Marino, R. C. Pooser, V. Boyer, and P. D. Lett, Nature (London) **457**, 859 (2009).
[25] J. Jing, C. Liu, Z. Zhou, Z. Y. Ou, and W. Zhang, Appl. Phys. Lett. **99**, 011110 (2011).
[26] A. M. Marino, N. V. Corzo Trejo, and P. D. Lett, Phys. Rev. A **86**, 023844 (2012).
[27] F. Hudelist, J. Kong, C. Liu, J. Jing, Z. Y. Ou, and W. Zhang, Nat. Commun. **5**, 3049 (2014).
[28] B. E. Anderson, P. Gupta, B. L. Schmittberger, T. Horrom, C. Hermann-Avigliano, K. M. Jones, and P. D. Lett, Optica **4**, 752 (2017).
[29] S. Liu, Y. Lou, J. Xin, and J. Jing, Phys. Rev. Appl. **10**, 064046 (2018).
[30] R. C. Pooser and B. Lawrie, Optica **2**, 393 (2015).
[31] X. Pan, S. Yu, Y Zhou, K. Zhang, K. Zhang, S. Lv, S. Li, W. Wang, and J. Jing, Phys. Rev. Lett. **123**, 070506 (2019).
[32] Z. Qin, L. Cao, H. Wang, A. M. Marino, W. Zhang, and J. Jing, Phys. Rev. Lett. **113**, 023602 (2014).
[33] Z. Qin, L. Cao, and J. Jing, Appl. Phys. Lett. **106**, 211104 (2015).
[34] W. Wang, L. Cao, Y. Lou, J. Du, and J. Jing, Appl. Phys. Lett. **112**, 034101 (2018).
[35] L. Cao, J. Qi, J. Du, and J. Jing, Phys. Rev. A **95**, 023803 (2017).
[36] L. Cao, W. Wang, Y. Lou, J. Du, and J. Jing, Appl. Phys. Lett. **112**, 251102 (2018).
[37] H. Wang, C. Fabre, and J. Jing, Phys. Rev. A **95**, 051802(R) (2017).
[38] S. Liu, H. Wang, and J. Jing, Phys. Rev. A **97**, 043846 (2018).
[39] S. Liu, Y. Lou, and J. Jing, Opt. Express **27**, 37999 (2019).
[40] K. Zhang, W. Wang, S. Liu, X. Pan, J. Du, Y. Lou, S. Yu, S. Lv, N. Treps, C. Fabre, and J. Jing, Phys. Rev. Lett. **124**, 090501 (2020).
[41] S. Li, X. Pan, Y. Ren, H. Liu, S. Yu, and J. Jing, Phys. Rev. Lett. **124**, 083605 (2020).
[42] A. Furusawa, J. L. Sørensen, S. L. Braunstein, C. A. Fuchs, H. J. Kimble, and E. S. Polzik, Science **282**, 706 (1998).
[43] N. Otterstrom, R. C. Pooser, and B. J. Lawrie, Opt. Lett. **39**, 6533 (2014).
[44] A. Ferreri, M. Santandrea, M. Stefszky, K. H. Luo, H. Herrmann, C. Silberhorn, and P. R. Sharapova, Quantum **5**, 461 (2021).
[45] Y. Fang and J. Jing, New J. Phys. **17**, 023027 (2015).
[46] S. Liu, Y. Lou, and J. Jing, Phys. Rev. Lett. **123**, 113602 (2019).
[47] H. Chen and J. Zhang, Phys. Rev. A **79**, 063826 (2009).
[48] J. A. Levenson, I. Abram, T. Rivera, and P. Grangier, J. Opt. Soc. Am. B **10**, 2233 (1993).
[49] H. Wang, K. Zhang, Z. Ni, and J. Jing, Opt. Express **28**, 10633 (2020).
[50] H. A. Bachor and T. C. Ralph, *A Guide to Experiments in Quantum Optics* (Wiley-VCH, Weinheim, 2004).
[51] C. M. Caves, Phys. Rev. Lett. **45**, 75 (1980).
[52] C. F. McCormick, A. M. Marino, V. Boyer, and P. D. Lett, Phys. Rev. A **78**, 043816 (2008).
[53] S. Liu, Y. Lou, and J. Jing, Opt. Express **29**, 38971 (2021).
[54] Q. Wang, Y. Tian, W. Li, L. Tian, Y. Wang, and Y. Zheng, Phys. Rev. A **103**, 062421 (2021).
[55] Y. Wu, Q. Wang, L. Tian, X. Zhang, J. Wang, S. Shi, Y. Wang, and Y. Zheng, Photonics Res. **10**, 1909 (2022).
[56] S. Shi, L. Tian, Y. Wang, Y. Zheng, C. Xie, and K. Peng, Phys. Rev. Lett. **125**, 070502 (2020).
[57] Q. Wang, Y. Wang, X. Sun, Y. Tian, W. Li, L. Tian, X. Yu, J. Zhang, and Y. Zheng, Opt. Lett. **46**, 1844 (2021).
[58] Q. Wang, W. Li, Y. Wu, W. Yao, F. Li, L. Tian, Y. Wang, and Y. Zheng, Phys. Rev. A **104**, 032419 (2021).
[59] W. Yang, S. Shi, Y. Wang, W. Ma, Y. Zheng, and K. Peng, Opt. Lett. **42**, 4553 (2017).
[60] W. Zhang, J. Wang, Y. Zheng, Y. Wang, and K. Peng, Appl. Phys. Lett. **115**, 171103 (2019).